Research Article

Chemical Review and Letters
journal homepage: www.chemrevlett.com
ISSN (online): 2645-4947(print) 2676-7279

Theoretical investigation of sulfur impurity on the structural, electronic and optical properties of C_3N monolayer

Erfan Cholaki[1], Borhan Arghavani Nia[1,*], Robab Mohammadi[2], Beheshteh Ajdari[3]

[1]*Department of Physics, Kermanshah Branch, Islamic Azad University, Kermanshah, Iran*
[2]*Department of Chemistry, Payame Noor University, PO box 19395-3697, Iran*
[3]*Department of Analytical Chemistry, Faculty of Chemistry and Petroleum Sciences, Bu-Ali Sina, University, Hamedan, 6517838695, Iran*

ARTICLE INFO

Article history:
Received 24 August 2024
Received in revised form 11 October 2024
Accepted 12 October 2024
Available online 25 October 2024

Keywords:
C_3N Monolayer,
Anisotropy,
Density Functional Theory,
Optical Properties.

ABSTRACT

In this article, structural, electronic and optical properties of monolayer doped with sulfur atom were investigated using density functional theory with WIEN2k computational code. The study of the electronic properties reveals that by replacing the sulfur atom with the nitrogen atom, the nature of the pure monolayer structure changes from semiconductor to metal. The examination of the optical properties in both x and z directions demonstrates the optical anisotropy of this structure. Due to the difference in the energy levels of the orbitals and the large size of the sulfur atom compared to the carbon and nitrogen atoms in the C3N structure, this atom acts as a disturbance factor causing a decrease in the degeneracy of the energy levels, so there is no sharp peaks corresponding to degeneracy transition in this structure.

1. Introduction

Graphene and its derivatives are groundbreaking materials with a two-dimensional hexagonal structure, offering exceptional electrical conductivity, strength, and flexibility. Their versatility and chemical modifiability enable applications in electronics, energy storage, sensors, biomedicine, and more. Ongoing research highlights their potential in advancing technology and solving global challenges [1]. In this structure, particles behave like Dirac mass-less fermions, leading to many suitable electrical properties making graphene a suitable candidate for the design and fabrication of future nanoelectronic components [2-4]. For this reason, scientists have expanded their research in the field of two-dimensional materials in recent years, and the results of these researches have led to the creation of new two-dimensional materials [5,6]. One of the notable points on two-dimensional materials is that their properties can be altered by applying changes such as absorption, impurity contamination, creating defects, or applying other physical properties [7-11]. The most important and practical method to adjust and control the electronic properties of nanomaterials is to replace the atom of that material with other atoms. Extensive studies have been reported on the structural properties of two-dimensional materials doped with different atoms [12-14].C_3N @pure monolayer is a non-magnetic semiconductor with a small gap of 3.9eV. Nitrogen-doped C_3N monolayer has a structure similar to graphene with a better performance than graphene, such as g-C_3N_4 and C_2N, both of which have been studied as the photocatalysts for the evaluation of hydrogen through dehydration [15,16]. Following the development of materials science, many new materials with suitable physical and chemical properties have been predicted for the design of required high-performance nanodevices. Vinada et al [17] reported new results for thin film materials that can be considered as promising candidates for various applications including optoelectronics, photocatalysts, gas sensors and light emitting diodes [18,19]. Two-dimensional carbon nitride materials have been widely used in many applications such as device fabrication, gas absorption, and separation

*Corresponding author; e-mail: b.arghavani@gmail.com
https://doi.org/ 10.22034/crl.2024.474907.1413

due to their high physical and chemical stability and excellent electronic properties. Laboratory research shows that two-dimensional carbon nitride materials have semiconductor properties, while it is predicted based on theoretical findings that these structures have semiconductor and insulator properties. However, few carbon nitride compounds have metallic and half-metallic properties [20,21]. Conducting scientific studies to find metallic or half-metallic carbon nitride has attracted the attention of researchers. In the present work, the basic method used in this simulation is first presented. The structural, electronic, and optical properties of sulfur-doped C_3N monolayer are investigated. The results provide a different strategy for realizing single atom doping, and they give a new insight into the structure and properties of sulfur atom.

2. Computational Details

Calculations of structural and electronic properties have been performed by the first principles method based on the density functional theory using the full potential linearized augmented plane wave method (FP-LAPW) [22]. For this purpose, WIEN2k code has been used with local density and generalized gradient approximations and correlation-exchange function. The pure C_3N unit cell is a hexagonal structure with the number of 6 carbon atoms and 2 nitrogen atoms, which crystallizes in the PGnmm-191 space group. The C_3N @pure monolayer is a non-magnetic semiconductor with a small gap of 0.5 eV, which is in good agreement with previous works [23,24]. The value of RKmax is equal to 8,

Gmax is equal to 12, and the Kpoint is also equal to 200. In order to determine the impurity concentration, a supercell was created with dimensions of 2x2x2, containing 64 atoms, of which 48 are carbon atoms and 16 are nitrogen atoms. For impurity, a nitrogen atom was removed and replaced with a sulfur atom; the impurity concentration is equal to 6%. Moreover, Kramers-Kronig relationships and RPA random phase approximation method are used to obtain the components of the complex dielectric function of this nanostructure.

3. Results and Discussion

3.1. Structural Properties

Lattice parameters are among the structural features of each crystal, which can be obtained in a state where the structure is at its minimum energy. Then, the energy curve of the whole unit cell is drawn for different lattice parameters to fit it with an equation of state, which is known as Murnaghan equation:

$$E(V) = E_0 + \left[B \times \frac{V}{B_0'} \times \left(\frac{1}{(B_0' - 1)} \times \left(\frac{V_0}{V}\right)^{B_0'} + 1\right) - B \times \frac{V_0}{(B_0' - 1)}\right] \quad (1)$$

$$Pressure = \frac{B}{B_0'} \times \left[\left(\frac{V_0}{V}\right)^{B_0'} - 1\right] \quad (2)$$

where B is the bulk modulus, B' is the derivative of the bulk modulus, and V is the cell volume. This curve has a parabolic behavior giving the minimum point of the curve, the minimum level, and as a result, the equilibrium lattice parameter. The values of these parameters are listed in Table 1.

Table 1: Total energy (E), equilibrium volume (V), bulk modulus (B), derivative of bulk modulus (' B), for C_3N @S monolayer

Parameter	E (Ry)	V (Bohr^3)	B (Gpa)	B
C_3N@S	-1364.58	1491	415.05	-6.97

The atomic structure of the doped S monolayer, which is a planar hexagonal lattice, is shown in (Scheme 1). C_3N @S lattice constants and bond lengths are listed in Table 2.

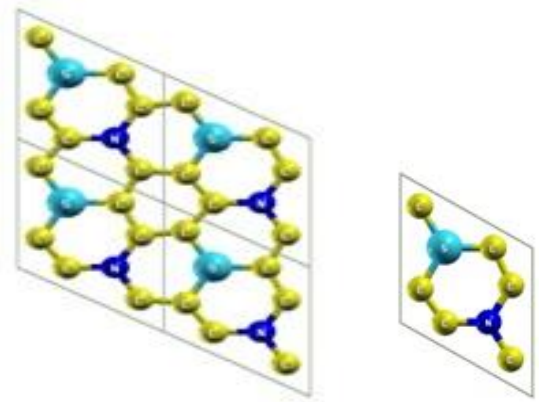

Scheme 1. C_3N @S primary unit cell

Table 2: Lattice constants, bond lengths and adhesion energy, respectively

Structure	Lattice Parameter (bohr)	Bond Length (Å)	Ec (Kj/mol)
C3N@S	a= 9.39	N-C 1.433	-40.20
	b= 9.39	C-C 1.293	
		S-C 1.884	

As seen in Table 2, by doping S atom instead of N atom to this structure, the length of the bonds changes. The greater the radius of the doped atom compared to nitrogen,

the longer the bond length of the doped atom with the second neighboring atoms is, which this change in the structure causes changes in the physical properties of this material. In order to investigate the characteristics of this structure, its electronic structure calculations are optimized, as shown in (Scheme 2).

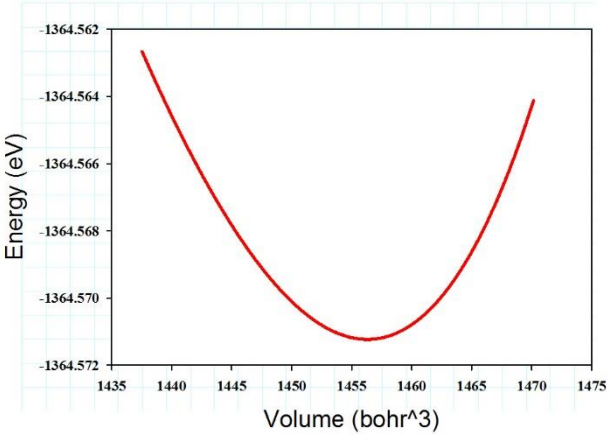

Scheme 2. Energy change curve versus volume

To check the chemical stability of this structure, its adhesion energy is calculated, which is obtained from the following equation

$$E_{(c)} = -\frac{E_{tot}^{C3N@S} - [N_C E_C^{single} + N_N E_N^{single}]}{N_C + N_N} (3)$$

where E_{tot} is the total energy calculated for the C_3N@S structure, and E_C and E_N are the energies of carbon and nitrogen atoms, respectively. N_C and N_N indicate the number of carbon and nitrogen atoms. The results of this calculation are listed in Table 2. As can be seen, the obtained negative value is a proof of the thermodynamic stability of this structure. The phonon calculations of this structure have already been performed, revealing that this structure in its pure state does not have any negative branches, so it is completely stable [25].

3.2. Electronic Properties

The density of states of the doped structure is illustrated in (Scheme 3). With doping S atom, the diagram of the density of electron states at the Fermi level is non-zero. In addition, the electron states of the conduction and valence bands overlap in the Fermi level, and the energy gap is zero. The diagram of electron states in up and down spin states intersects the Fermi level, so metallic characteristics are obtained due to doping C3N structure with sulfur atom. Apparently, the density of electron states for up and down spins is equal, indicating that this structure is non-magnetic. Additionally, according to this fact that, at high energies, the number of states and the probability of the presence of electrons is raised in relation to the Fermi and valence regions, the material acquires a strong metallic property.

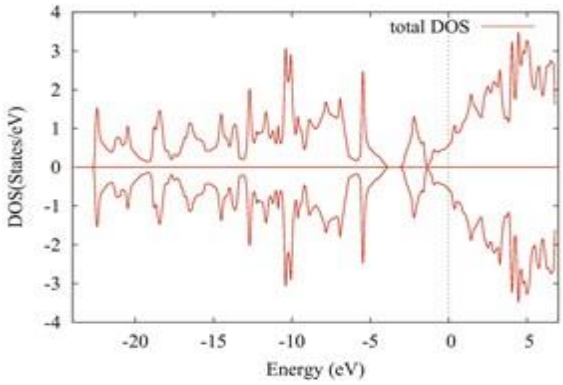

Scheme 3. Density of states of C_3N@S for up and down spins

In order to examine the electronic properties and the type of bonds, as well as the effect of guest atoms, especially on the Fermi level, the partial density of states diagram of the constituent atoms for this structure can be seen in (Scheme 4). For the C_3N@S structure, the contribution of the guest atom to energies higher than the Fermi level is more of two other atoms, and the share of P orbital is more than that of S orbital of the guest atom.

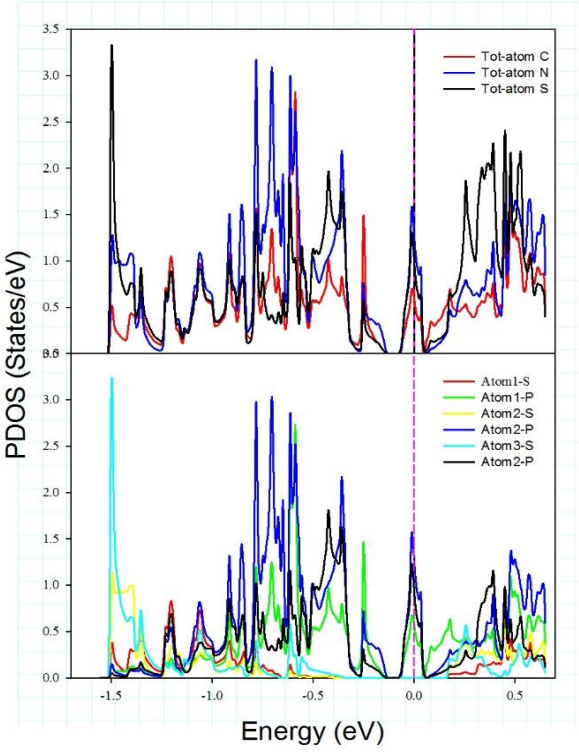

Scheme 4. Partial density of states diagram

The band structure diagram is depicted in (Scheme 5). With the obtained optimal parameters, the energy bands are obtained using the PBE-GGA approximation. By adding impurity of S atom, there is no energy gap. Furthermore, according to the valence band, it intersects the Fermi level, so the diagram displays that this structure is metallic. The results obtained from the band structure are completely consistent with the results of the density of states.

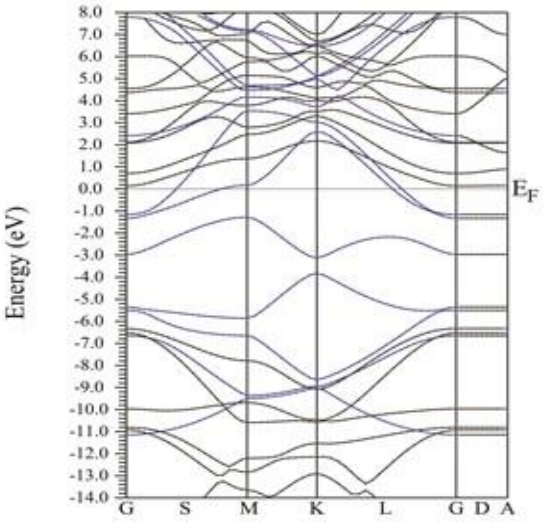

Scheme 5. Band structure for C_3N @S

3.3. Optical Properties

After calculation of the electronic structures, optical properties like imaginary and real parts of the dielectric function, electron energy loss function, refraction index and absorption coefficient of C_3N@Shave been studied by using the random phase approximation (RPA) approach.
The imaginary part of the dielectric function, ε_2, canbe obtained from the momentum matrix elements between the occupied and unoccupied wave functions [26]:

$$Im\varepsilon_{\alpha\beta}^{\{inter\}}(\omega) = \frac{\hbar^2 e^2}{\pi m^2 \omega^2}\sum_n \int dk \langle \psi_k^{c_n} | P^{\alpha} | \psi_k^{v_n} \rangle \langle \psi_k^{v_n} | P^{\beta} | \psi_k^{c_n} \rangle \delta(E_k^{c_n} - E_k^{v_n} - \omega) \quad (4)$$

The absorption spectrum is proportional to the sum over interband transitions from occupied valence states $\psi_k^{v_n}$ to empty conduction states $\psi_k^{c_n}$ over the first Brillouin-zone k points, where $E_k^{c_n}$ and $E_k^{v_n}$ are conduction band (CB) and valance band (VB), respectively. The real part $\varepsilon_1(\omega)$ can be evaluated from $\varepsilon_2(\omega)$ using the Kramer-Kronig relations:

$$Re\varepsilon_{\alpha\beta}^{\{inter\}}(\omega) = \delta_{\alpha\beta} + \frac{2}{\pi} P \int_0^{\infty} \frac{\omega Im\varepsilon_{\alpha\beta}(\omega')}{(\omega')^2 - \omega^2} \quad (5)$$

The knowledge of $\varepsilon_1(\omega)$ and $\varepsilon_2(\omega)$ allows the calculation of other optical constants such as energy loss function$L(\omega)$, refraction coefficient$n(\omega)$ and absorption coefficient *α(ω)*. $L(\omega)$,$n(\omega)$and $\alpha(\omega)$ can be computed from the complex dielectric function,$\varepsilon(\omega)$, through the following relations [27-29]:

$$L_{ij}(\omega) = -Im\left(\frac{1}{\varepsilon_{ij}(\omega)}\right) = \frac{\varepsilon_{ij}''(\omega)}{\varepsilon_{ij}'^2(\omega) + \varepsilon_{ij}''^2(\omega)} \quad (6)$$

$$n_{ij}(\omega) = \sqrt{\frac{\left|\varepsilon_{ij}(\omega) + Re\varepsilon_{ij}(\omega)\right|}{2}} \quad (7)$$

$$a_{\alpha\beta}(\omega) = \frac{2\omega k_{\alpha\beta}(\omega)}{c} \quad (8)$$

where c is the speed of light in vacuum and $k_{\alpha\beta}$ is imaginary part of the complex refractive index, known as the extinction index. It is given by the following relations

$$k_{\alpha\beta}(\omega) = \sqrt{\frac{\left|\varepsilon_{\alpha\beta}(\omega) - Re\varepsilon_{\alpha\beta}(\omega)\right|}{2}} \quad (9)$$

The real and imaginary parts of the dielectric function are given in (Scheme 6).

Owing to the crystal symmetry of this compound, its optical response is completely symmetrical in both x and y directions, and for the graphs, the x direction is only considered. However, the optical behavior along the z direction is different from the other two directions. As can be seen from the Scheme, the difference in the x- and z-direction graphs represents the anisotropy of the crystal, meaning that the crystal behavior will be different for incident photons in these directions. In the areas where the real part of the dielectric function has a peak, the structure exhibits the highest transparency, as well as the lowest absorption and conductivity.
When the S atom is doped in the C_3N structure, this atom acts as a disturbance factor and causes the energy levels to become misaligned because of the difference in the energy levels of the orbitals and the large size of the sulfur atom compared to the carbon and nitrogen atoms in the C_3N structure. There are no sharp peaks related to the degeneracy transition in this structure.
The static value of the real part tends to negative infinity in the x direction, and this value is 1.36 in the z direction, indicating that by changing the angle of the incident light along the z direction, it has an approximately

semiconductor behavior while it behaves strongly metallic in the x direction.

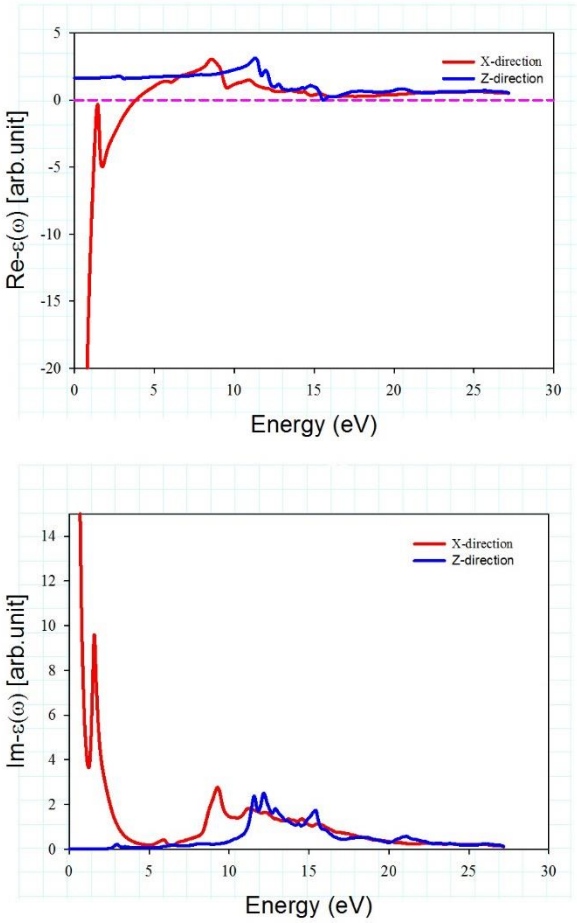

Scheme 6. The top image is the real part of the dielectric function in the X and Z directions, and the bottom image is the imaginary part of the dielectric function in the X and Z directions.

With the increase of photon energy, the maximum value is equal to 1.8 at the energy of 12 eV in the z direction. In the X direction, the real part is negative up to the range of 1 eV due to metallic behavior, and after that it has small fluctuations, the maximum of which is 3 at the energy of 2.8 eV. The imaginary part of the dielectric function has a zero value in the z direction at zero energy although it tends to the positive side of infinity in the x direction, exhibiting that the behavior of this structure is metallic. In the z direction up to the energy range of 2.5 eV, the imaginary value of the dielectric function is zero, indicating the energy gap in this range. By increasing the energy, this value escalates to reach its maximum value of 2 at the energy of 12 eV, representing semiconductor behavior from an optical point of view. In both directions, in the energy range of 2 to 15 eV, several peaks can be seen representing interband transitions, and from 16 eV onwards, a decrease can be observed in the transition. The metallic and semiconductor properties from an optical point of view in these two directions can be utilized. The absorption coefficient diagram is shown in (Scheme 7).

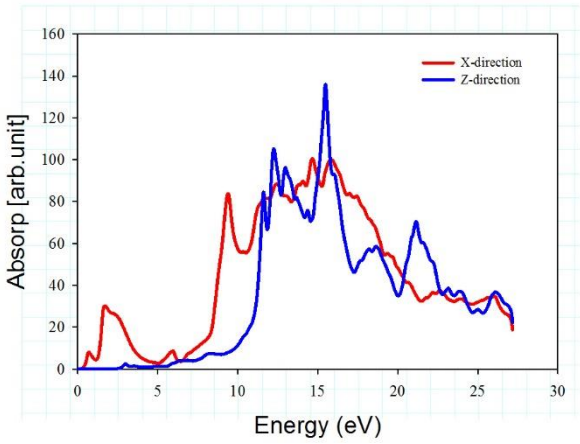

Scheme7. Absorption diagram in terms of energy in X and Z directions.

The absorption edges have occurred at energies of 0.5 and 3 eV in the x and z directions, respectively. Optical anisotropy is evident in the behavior of the absorption spectrum. In the x direction, peaks are seen in the range of the visible light region at energies of 1 and 3 eV while in the z direction, no peaks are observed in the visible light region.Variations of electron energy loss function are presented in (Scheme 8) in terms of incident photonenergy for x and z directions.

The electron energy loss spectrum for both x and z directions starts at zero electron volt energies. In this regard, a large peak is detected at low energies in the x direction, which is related to optical transitions. At energies that are the function of maximum loss, the intensity of the inter-band transition is minimal. Conversely, there is the highest energy loss in the energy range of 1 to 3 eV, and the intensity of the interband transition is zero. The sudden change of slope, occurred in the real part of the dielectric function in the z direction, causes peaks in the part of the energy loss function. There is a gap in the diagram of the imaginary part in the z direction in the visible light range, confirming the behavior of the energy loss diagram in the z direction. The broad peaks, seen at higher energies in the energy range of 7 to 22 eV in the x direction and 12 to 20 eV in the z direction, can be related to Plasmon peaks of the $\pi+\sigma$ electrons that the intraband interaction effects also play an important role in the energy loss function in the presence of impurity. In the z direction, materials behave as semiconductors at frequencies lower than the Plasmon frequency, and as metals at higher frequencies. The most

prominent peak in the energy loss function is known as the Plasmon peak, representing the collective excitation of the electron charge density in the crystal. In the x direction, the prominent peaks are observed in the energy range of 3 eV while it can be seen in the energy range of 16 eV in the z direction. The best optical response in the X direction is in the IR region.

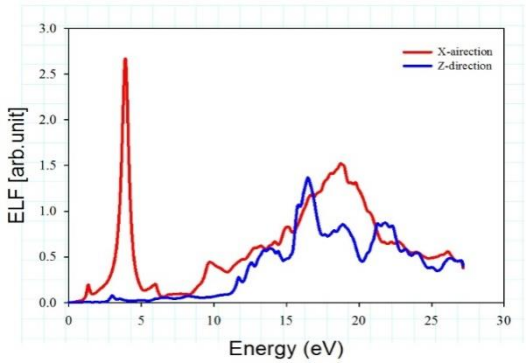

Scheme 8. Energy loss function diagram in terms of energy in X and Z directions.

4. Conclusion

In summary, a first-principles simulation is studied to investigate the structural properties of C_3N@S. The results of the calculations reveal that the C_3N monolayer doped with sulfur atom has metallic and non-magnetic properties. Due to the anisotropy of this structure, the maxima of the refractive index are different in different directions, and this anisotropy and the incompatibility of the graphs cause birefringence in this structure. The best optical response in the X direction is in the IR region.The presented electronic and optical results of the studied structure show that it is very useful for the design of advanced nanoelectronic nano-systems and energy conversion (batteries). These results provide a different strategy for realizing single-atom impurity, and they reveal new insights into the structure and properties of the sulfur atom.

References

[1] a) P. Wu, P. Du, H. Zhang, and C. Cai, "Graphyne-supported single Fe atom catalysts for CO oxidation", Physical Chemistry Chemical Physics, 17(2),(2014) 1441–1449. b) E. Vessally, S. Soleimani-Amiri, A. Hosseinian, L. Edjlali, A. Bekhradnia, A comparative computational study on the BN ring doped nanographenes, Applied Surface Science, 396 (2017) 740-745. c) S. Esfahani, J. Akbari, S. Soleimani-Amiri, Adsorption of Ibuprofen by an Iron-doped Silicon Carbide Graphene monolayer: DFT exploration of drug delivery insights, International Journal of Nano Dimension, 15 (2024) 63-71. d) E. Vessally, M. R. Ilghami, M, Abbasian, Investigation the Capability of Doped Graphene Nanostructure in Magnesium and Barium Batteries with Quantum Calculations, Chem. Res. Technol., 1 (2024) 10.2234/chemrestec.2024.436837.1007.

[2] a) B. Machado and P. Serp,"Graphene-basedmaterials for catalysis", Catal. Sci. Technol, 2, (2012)54–75. b) B. Hashemzadeh, L. Edjlali, P. Delir Kheirollahi Nezhad, E. Vessally, A DFT studies on a potential anode compound for Li-ion batteries: Hexa-cata-hexabenzocoronene nanographen, Chemical Review and Letters 4(4) (2021) 232-238. c) E. Vessally, S.A. Siadati, A. Hosseinian, L. Edjlali, Selective sensing of ozone and the chemically active gaseous species of the troposphere by using the C20 fullerene and graphene segment, Talanta 162 (2017) 505-510. d) A. Karbakhshzadeh, S. Majedi, V. Abbasi, Computational investigation on interaction between graphene nanostructure BC3 and Rimantadine drug: Possible sensing study of BC3 and its doped derivatives on Rimantadine, J. Chem. Lett. 3 (2022) 108-113.

[3] a) S. Esfahani, J. Akbari, , S. Soleimani-Amiri, M. Mirzaei, &A.G. Gol, Assessing the drug delivery of ibuprofen by the assistance of metal-doped graphenes: insights from density functional theory. Diamond and Related Materials, 135, (2023). 109893. b)

[4] M.R.Poor Heravi, B. Azizi, E.Abdulkareem Mahmood, A. G. Ebadi, M.J. Ansari, &S. Soleimani-Amiri, Molecular simulation of the paracetamol drug interaction with Pt-decorated BC3 graphene-like nanosheet. Molecular Simulation, 48(6),(2022)517–525.

[5] A. Castro, H. Neto, F. Guinea, N.M.R Peres., K .S .Novoselov , and A.K.Geim., "Theelectronic properties of graphene", Rev. Mod. Phys, 81(1), (2009)109–162.

[6] L. Adamska, and S. Sharifzadeh, "Fine Tuning the Optoelectronic Properties of Freestanding Borophene by Strain", ACS Omega,2,(2017) 8290-8299

[7] S. Yang, W. Li, C. Ye, G. Wang, H. Tian, C. Zhu, P.He, G.Q Ding, X.M. Xie, Y. Liu, Y. Lifshitz, S. Lee, Z. Kang, and Jiang M, "C_3N —A 2D crystalline, hole-free, tunable-narrow-bandg
ap semiconductor with ferromagnetic properties." Advanced Materials, 29,(2017) 1605625.

[8] M. Makaremi, B. Mortazavi, and C. Singh, “Adsorption of Metallic, Metalloidic, and21 Nonmetallic Adatoms on Two-Dimensional C_3N”, J. Phys. Chem. C,121 (2017)18575 -18583.

[9] S.J.E. Koohbanani, S.A. Ahmadi, D. Ghazanfari, &E.Sheikhhosseini, Theoretical investigation of fullerene (C_{60}) as nano carrier for anti-cancer drug Axitinib. Carbon Trends, 14, (2024). 100332.

[10] A. Safamanesh, S. A. Ahmadi, E. Sheikhhosseini, &D. Ghazanfari, Theoretical Study of Adsorption of Alprazolam on Functionalized Fullerene as a Nano Drug Carrier. Iranian Journal of Chemistry and Chemical Engineering, 43(2), (2024). 652-658.

[11] S. Tavakoli, S. A.Ahmadi, D.Ghazanfari, , & E. Sheikh hosseini, Theoretical investigation of functionalized fullerene nano carrier drug delivery of fluoxetine. Journal of the Indian Chemical Society, 99(7), (2022) 100561.

[12] Z. Nazar Ali, , S. A. Ahmadi, D.Ghazanfari, E. Sheikhhosseini, &R. Razavi,. Investigation of Flutamide @Ethyleneimine as Drug Carrier by Nanocone and Nanotube Theoretically. Iranian Journal of Chemistry and Chemical Engineering, 41(10),(2022)3275-3281.

[13] X. Rao, Q. Si, T. Shi, X. Han, and S. Ma, "Fe-doped C_3N monolayer as a promising SAC for CO oxidation with low temperature and high reactivity", Computational and Theoretical Chemistry,55(2021)1194, 113080.

[14] M. Bagheri, "Electrical and mechanical properties of a fully hydrogenated two-dimensional polyaniline sheet", Computational Materials Science,153, (2018)126-133,

[15] M. Bagheri, and S. Izadi, "Polyaniline (C3N) nanoribbons: Magnetic metal, Semiconductor, and Half-Metal", Applied physics124, (2018) 84304.

[16] J. Xu, J. Mahmood, Y. Dou, S. Dou, F. Li, L. Dai, and J.B. Baek, , "2D frameworks of C_2N and C_3N as new anode materials for lithium-ion batteries", Advanced Materials, 29(34), (2017) 1702007,

[17] B. He, J. Shen, D. Ma, Z. Lu, and Z. Yang, "Boron-Doped C_3N Monolayer as a Promising Metal-Free Oxygen Reduction Reaction Catalyst: A Theoretical Insight", J. Phys. Chem. C, 122, (2018)20312–20322.

[18] Q. Wu, Wongwiriyapan, W. Park J.H. Sangwoo, Park, S.J. Jung, T. Jeong, S. Lee, H.L. Young, and Y.J. Song, "In situ chemical vapor deposition of graphene and hexagonal boron nitride heterostructures", Current Applied Physics16(9),(2016) 1175-1191.

[19] A.A. Tedstone, D.J. Lewis, R. Hao, S.M. Mao, P. Bellon, R.S Averback, et al., "Mechanical Properties of Molybdenum Disulfide and the Effect of Doping: An inSitu TEM Study", ACS Appl. Mater. Interfaces, 7,37 , (2015) 20829–20834.

[20] E. Cholaki, B Arghavani Nia, S Rezaee and S Parsamehr Calculation of structural, electronic, magnetic and optical properties of C_3N monolayer substituted with magnesium, Eur. Phys. J. Appl. Phys. 99(2024)5.

[21] F.Yahyazadeh, D. Ghazanfari, , S. A.Ahmadi, &M. R. Akhgar,Adsorption of Nefazodone on single-wall Carbon Nanotube as an antidepressant drug delivery: A DFT Study. Carbon Trends, (2024)100394.

[22] K.EinalipourEshkalak, S.Sadeghzadeh, and F. Molaei, "Interfacial Thermal Resistance Mechanism for the Polyaniline (C3N)–Graphene Heterostructure", J. Phys. Chem. C,124,(2020)14316–14326.

[23] A.K. Geim and I.V. Grigorieva, "Van der Waals heterostructures", Nature, 499,)2013(419-425

[24] E.Cholaki, B. Arghavani Nia, & M. H.Sahafi,. Investigation of Thermoelectric, Dynamical, Electron and Optical Properties of C_3N Monolayer Using First Principles Calculations. Iranian Journal of Applied Physics, 14(1), (2024) 7-24.

[25] V. Babar, S. Sharma, and U. Schwingenschlögl. Highly sensitive sensing of NO and NO_2 gases by monolayer C_3N. Advanced Theory and Simulations,1 (2018).

[26] Y. Gao, H. Wang, M. Sun, Y. Ding, L. Zhang, Q.Li, & Zhang, First-principles study of phononic thermal transport in monolayer C3N: A comparison with graphene. JarXiv: Materials Science:17, (2017) 09.08821.

[27] R.Ghiasi, V.Daneshdoost, & R. Tale,Exploring of structural, electronic, and optical properties of transition metal doped C20 clusters. International Journal of Nano Dimension (Int. J. Nano Dimens.) (2024).

[28] H. Asadzadeh, R. Ghiasi, M. Yousefi, &S. Baniyaghoob, C-PCM study on the electronic and optical properties of Fe (CO) 4B 12N 12 complexes. Main Group Chemistry, 22(1),(2023)31-41.

[29] R.Ghiasi, M. Rahimi, , &P.R. Jamaat, Quantum Chemical Study of the Effect of Solvent on Structure, Electronic Properties, and Electronic Spectrum of the Carbyne Complex trans-[ClRu (PH 3) 4 (≡ C–CH= CMe 2)] 2+. Russian Journal of Inorganic Chemistry, 65, (2020) 69-75.